Journal of Hazardous Materials 211–212 (2012) 255–265

Contents lists available at ScienceDirect

Journal of Hazardous Materials

journal homepage: www.elsevier.com/locate/jhazmat

N_2O decomposition by mesoporous silica supported Rh catalysts

Murid Hussain[a,b], Debora Fino[a], Nunzio Russo[a,*]

[a] Department of Materials Science and Chemical Engineering, Politecnico di Torino, Corso Duca degli Abruzzi 24, 10129 Torino, Italy
[b] Department of Chemical Engineering, COMSATS Institute of Information Technology Lahore Campus, M.A. Jinnah Building, Defence Road, Off Raiwind Road, Lahore-54000, Pakistan

ARTICLE INFO

Article history:
Received 13 April 2011
Received in revised form 4 July 2011
Accepted 7 August 2011
Available online 25 August 2011

Keywords:
Mesoporous silica
Rh catalyst
Dispersion
N_2O
Decomposition

ABSTRACT

Nitrous oxide (N_2O), a greenhouse gas produced by nitric acid and adipic acid plants, damages the ozone layer and causes many environmental problems. The potential of MCM-41, SBA-15-Conventional (SBA-15-C), SBA-15-Spherical (SBA-15-S) and KIT-6 supported Rh catalysts has been explored at specific conditions for N_2O decomposition in order to investigate the characteristics of new catalyst supports (SBA-15-S, KIT-6) for this application. A Rh metal loading of 1 wt% was impregnated to synthesize mesoporous silica supported Rh catalysts. The catalysts were characterized by scanning electron microscope (SEM), energy dispersive X-ray spectroscopy (EDX), X-ray diffraction (XRD), N_2 adsorption/desorption, X-ray photoelectron spectroscopy (XPS), transmission electron microscopy (TEM) and CO-chemisorption techniques. Of all the catalysts, Rh/SBA-15-S not only showed the highest activity, but also the best strength against ageing impact, O_2 inhibiting effect and long-term stability. The higher metal dispersion due to the smaller Rh particle size and a greater formation of Rh^{+1} than Rh^0 or Rh^{+3} on SBA-15-S compared to the other supports, favoured a higher N_2O decomposition. The larger pore size of SBA-15-S in Rh/SBA-15-S might favour a better Rh access, diffusion and dispersion and lead to higher activity. The higher long-term stability of Rh/SBA-15-S, with preserved support characteristics, than the other supports indicates its significance.

1. Introduction

Nitrous oxide (N_2O) is an important component of the earth's atmosphere that has gained significant attention of late due to its environmental effects [1]. Due to its long life, of approximately 150 years, in the atmosphere, it is a potent greenhouse gas (ca. 310 and 21 times greater warming potential than CO_2 and CH_4, respectively) and is involved in the depletion of stratospheric ozone [1–5]. N_2O is produced by both natural and anthropogenic sources. Biological processes in soils and oceans are the primary natural sources of N_2O. The anthropogenic sources include agriculture (fertilizer production), nitric acid production, adipic acid production, fossil-fuel combustion (stationary and mobile), biomass combustion and sewage treatments [4]. Nitric acid production is currently believed to be the largest industrial source of N_2O emissions [6]. Thus, a reduction in anthropogenic N_2O emissions is urgently required, and catalytic direct N_2O decomposition is considered the most effective and economic method to achieve this target [7].

A large number of catalysts, such as metal oxides, mixed oxides, perovskite-type oxides, hydrotalcites, and transition metal exchanged zeolites are known to be capable of decomposing N_2O to its elements at elevated temperatures [8–18]. Rhodium and iridium oxides have shown the highest activity for N_2O decomposition and the order is: $Rh_2O_3 > IrO_2 > CaO > CuO > SrO > HfO_2 \gg Fe_2O_3 > NiO > ThO_2 > SnO_2 > CeO_2 \gg MgO > Cr_2O_3 > ZnO > Ga_2O_3 > BeO > Al_2O_3 \gg TiO_2$ [19]. However, the disadvantages of metal oxides and mixed metal oxides as catalysts are due above all to their low surface areas.

ZSM-5, which is the most widely used zeolite, has mostly been used for N_2O decomposition in metal supported catalysts. Rh and Ru have been reported [8] to be the most active metals; the order of the catalyst activity is as follows: Rh, Ru > Pd > Cu > Fe > Pt > Ni > Mn. However, the exchange capacity of metals in zeolite pores is not high, due to its microporosity and low surface area, hence the application of zeolites is limited as support for the metallic component for N_2O decomposition catalysts. Catalyst supports with a high surface area are more attractive for practical applications since the active catalyst component can be highly dispersed on their surfaces [8].

The discovery of ordered mesoporous molecular sieves has sparked interest throughout the scientific community. These mesoporous silicas, first discovered by Mobil researchers, have a high surface area, pore volume and a narrow pore size distribution as compared with conventional zeolites and alumina materials. Because of these interesting properties, these materials played a role in heterogeneous catalysis as supports for metal oxides and metal catalysts for many types of reaction [20].

* Corresponding author. Tel.: +39 011 0904710; fax: +39 011 0904699.
E-mail address: nunzio.russo@polito.it (N. Russo).

0304-3894/$ – see front matter © 2011 Elsevier B.V. All rights reserved.
doi:10.1016/j.jhazmat.2011.08.024

Mesoporous silica materials are interesting catalyst supports for metal oxides and metals, due to a combination of good accessibility, uniform pore size and high surface area. Mobil composition of matter-41 (MCM-41) has a 2-dimensional (hexagonal p6 mm) pore structure with characteristics of high surface area, pore volume and confined pore size. It has been already proved to be an effective support for different metals and metal oxides in many applications [6,8,20]. The disclosure of Santa Barbara amorphous-15 (SBA-15) with 2-dimensional (large pore hexagonal p6mm) structure connected with small micropores, sparked considerable interest for its larger pore size, thicker wall and better stability than MCM-41. The most common morphology of SBA-15 is fiber-like several tens of micrometers in length is considered here as SBA-15-Conventional (SBA-15-C) and has already several applications [21,22]. Also, an effort has already been made in this regard to use SBA-15-C as a catalyst support for N_2O decomposition [6]. However, a spherical shaped SBA-15 (SBA-15-S) is used in the present study with much larger pore size and uniform shape in order to have better access and accessibility of metals and transportations of reactants and products. Korea Advanced Institute of Science and Technology-6 (KIT-6) silica is another charming material with 3-dimensional (large-pore gyroid cubic *Ia*3*d*) pore structure which has already received attention of many researchers for various application [21,23].

SBA-15-S and KIT-6 have here been used for the first time as supports for Rh catalysts for N_2O decomposition and they have been compared with MCM-41 and SBA-15-C in order to achieve a long lasting, stable and more active catalyst for N_2O decomposition. The influence of different pore structure and size of these mesoporous support materials on metals have been analyzed. As already mentioned, Rh was chosen due to its reported higher activity and it was impregnated by means of the incipient wetness method. A series of Rh oxides, supported on these mesoporous silicas, have been investigated for N_2O decomposition. Rh dispersion, particle size, and the different oxidation states of Rh on MCM-41, SBA-15-C, SBA-15-S, and KIT-6 supports have been compared in order to establish the effect of the support on N_2O abatement.

2. Experimental

2.1. Materials

Reagent grade cetyltrimethyl ammonium chloride (CTACl, 25 wt%, Aldrich), Pluronic P123 (P123, Aldrich), hydrochloric acid (HCl, 37%, Sigma Aldrich), tetraethyl orthosilicate (TEOS, 98%, Aldrich), potassium chloride (KCl, 99%, Sigma Aldrich), mesitylene (Aldrich), 1-butanol (99.5%, Fluka), and rhodium nitrate (Aldrich) were used directly without any further purification.

2.2. Synthesis of mesoporous silica supports

An MCM-41 support was hydrothermally synthesized with a CTACl surfactant according to the procedure already reported in Ref. [20]. The synthesized MCM-41 was dried and calcined at 550 °C for 5 h for further use.

SBA-15-C was synthesized according to the method reported in Ref. [21]. 2 g of P123 was dissolved in 15 g of deionised water and 80 g of 2 M HCl solution. Then, 4.25 g of TEOS was added and this mixture was stirred for 5 min and kept at 35 °C for 1 day, and this was then followed by ageing at 100 °C for another 24 h. Finally, it was filtered, dried and calcined at 550 °C for 5 h so that it could be used as a support.

SBA-15-S was obtained according to the procedure reported by Wang et al. [22]. The molar ratio of the reactants was 1TEOS:0.017P123:0.6 mesitylene:*x*KCl:5.85 HCl:165 H_2O, where x = KCl/TEOS molar ratio. 4 g of P123 and a certain amount of KCl (x = 2) was dissolved in 120 g of H_2O and 23.6 g of concentrated HCl at room temperature until the solution became transparent, then 3 g of mesitylene was added. After stirring for 2 h, 8.5 g of TEOS was added dropwise and stirred vigorously for 10 min. The mixture was then kept under static conditions at 35 °C for 1 day, followed by another 24 h at 100 °C. The resultant precipitate was filtered, washed, dried and calcined at 550 °C for 5 h so that it could be used as a support.

Finally, KIT-6 support material was synthesized according to the procedure reported in literature [23]. 6 g of P123 was dissolved in 217 g of distilled water and 11.8 g of concentrated HCl, and; 6 g of 1-butanol was added under stirring at 35 °C. After 1 h of stirring, 12.9 g of TEOS was added dropwise at 35 °C. The mixture was stirred for 24 h at 35 °C. The final solution was transferred to a Teflon bottle and heated at 100 °C for 24 h. The solid product obtained after the hydrothermal treatment was filtered, dried and calcined at 550 °C for 5 h so that it could be utilized as a support material.

2.3. Preparation of mesoporous silica supported Rh catalysts

Calcined MCM-41, SBA-15-C, SBA-15-S and KIT-6 supported Rh(1 wt%) catalysts were prepared by means of the incipient wetness method, using a rhodium nitrate precursor. After impregnation, each catalyst was dried in an oven at 100 °C for 12 h. The catalysts were then calcined at 550 °C for 6 h in the presence of air in order to obtain the supported rhodium oxide catalysts.

2.4. Characterization of the mesoporous silica supported Rh catalysts

Scanning electron microscopy (SEM) FEI Quanta Inspect 200 was used to observe the morphology of the synthesized mesoporous silicas. EDAX Genesis, with an SUTW detector equipped with the SEM equipment was used to carry out the energy dispersive X-ray (EDX) analysis in order to confirm the presence of silica and Rh.

Small angle X-ray diffraction (XRD) patterns were recorded to determine the different structures of the synthesized mesoporous silicas on an X'Pert Phillips diffractometer using Cu Kα radiation at 2θ = 0.1–6 or 10. Moreover, large angle XRD patterns of mesoporous silica supported Rh catalysts were obtained at 2θ = 10–70. The Brunauer–Emmett–Teller (BET) specific surface area (S_{BET}), pore volume (PV), average pore diameter (APD) and isotherms were measured on powders that had previously been outgassed at 150 °C, by means of N_2 sorption at 77 K on a Micromeritics ASAP 2020 instrument.

The XPS spectra were recorded using a PHI 5000 Versa Probe (USA) with a scanning ESCA microscope fitted with an Al monochromatic X-ray source (1486.6 eV, 25.6 W), a beam diameter of 100 μm, a neutralizer at 1.4 eV 20 mA, and a FAT analyzer mode. All the binding energies were referenced to the C1s peak at 284 eV of the surface adventious carbon. The individual components were obtained by curve fitting after proper subtraction of the baseline.

Transmission electron microscope (TEM) images were collected from the thin edges of the sample particles with a JEOL TEM 2010 (JEOL Ltd.) electron microscope, operating at 200 kV. High resolution field emission scanning electron microscopy (FE-SEM) images of Rh/SBA-15-S were obtained using a high-resolution FE-SEM instrument (LEO 1525) equipped with a Gemini field emission column.

Carbon monoxide chemisorption (CO-chemisorption) was conducted on the Rh supported catalysts in order to determine the metal dispersion using a Micromeritics ASAP 2020 instrument. The catalysts were evacuated at 150 °C for 5 h and this was followed by chemisorption of CO at 35 °C.

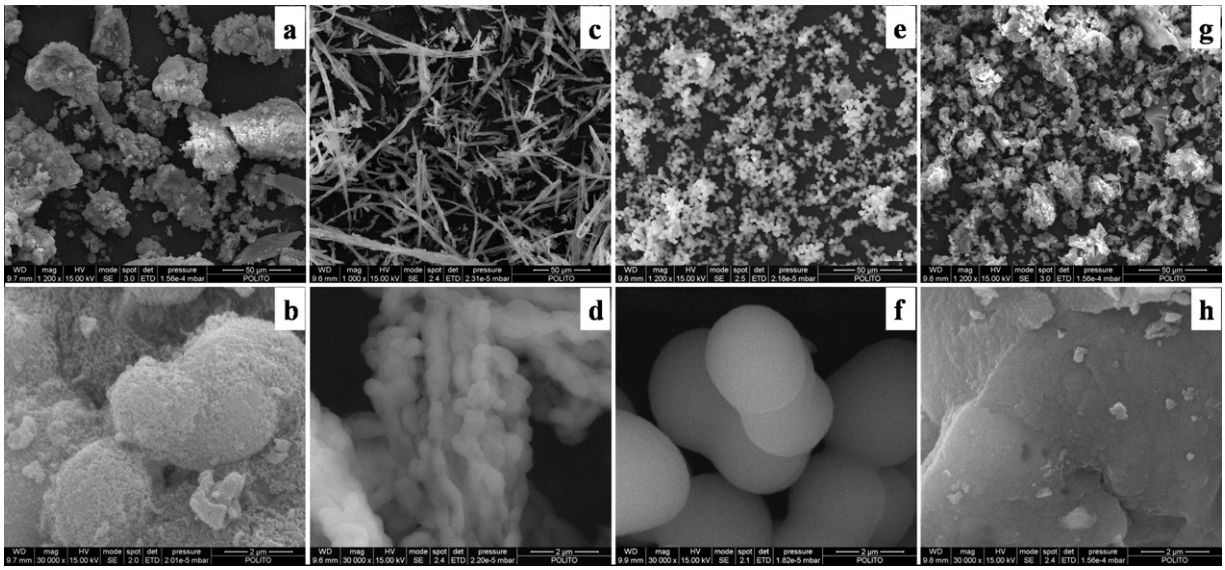

Fig. 1. SEM images of synthesized mesoporous silica support materials with different morphology: ((a), (b)) MCM-41, ((c), (d)) SBA-15-C, ((e), (f)) SBA-15-S, ((g), (h)) KIT-6.

2.5. N_2O decomposition reaction

The activity of the prepared catalysts was analyzed by temperature programmed reaction (TPR), according to a standard operating procedure: a gas mixture (1700 ppm N_2O; 0 or 5 vol. % O_2, He = balance) was fed at a constant rate of 100 mL/min, via a set of mass flow controllers to the catalytic fixed-bed micro reactor enclosed in a quartz tube placed in an electric oven. The tubular quarts reactor was loaded with 50 mg of catalyst pellets (250–425 μm). The W/F of the gases through the catalytic bed was 5×10^{-4} g min/N ml (GHSV = 26,500 h^{-1}). The reaction temperature was controlled through a PID-regulated oven and varied from 100 to 620 °C at a 5 °C/min rate. The outlet composition was monitored through a NO_x/N_2O NDIR (ABB) analyzer as a function of the bed temperature.

The catalytic activity was evaluated in terms of conversion of the N_2O, i.e. C_{N_2O} (%), according to the following equation:

$$C_{N_2O}(\%) = \frac{(C_{N_2O_{in}} - C_{N_2O_{out}})}{C_{N_2O_{in}}} \times 100$$

where $C_{N_2O_{in}}$ is the inlet concentration and $C_{N_2O_{out}}$ the outlet concentration of N_2O.

The temperature corresponding to half N_2O conversion (T_{50}) and full N_2O conversion (T_{90}) was taken as an index of the activity of the tested catalysts: the lower the T_{50} or T_{90} values, the more active the catalyst. In reduced catalytic test, the catalysts were first treated with H_2 at 400 °C for 3 h, cooled to room temperature and then the reaction was conducted in the absence of O_2.

3. Results and discussion

3.1. Characterization of the mesoporous silica supported Rh catalysts

3.1.1. SEM and EDX analysis

Mesoporous silica materials, with different morphologies and different characteristics, have been synthesized in order to use them as support materials for N_2O decomposition catalysts. Fig. 1 shows the SEM images of the calcined samples of the MCM-41((a) and (b)), SBA-15-C((c) and (d)), SBA-15-S((e) and (f)) and KIT-6((g) and (h)) materials. The images shown in Fig. 1(a and b) indicate that the pure siliceous MCM-41 particles are deposited together, and that the strongly compact agglomerates consist of individual spherical particles. However, bundles of SBA-15 with a short fiber-like morphology are shown in the SBA-15-C silica in Fig. 1(c and d). The large particles of SBA-15-C consisted of many smaller SBA-15-C particles, which were similar to macaroni in shape. SBA-15-S had a spherical morphology in agreement with Wang et al. [22]. SBA-15-S had well-dispersed microspheres with a limited dispersion of the particle size in the 2–3 μm range, together with a high yield of almost 100%. The morphology of KIT-6 is shown in Fig. 1(g and h) and is consistent with that shown in the literature [24].

EDX, a chemical microanalysis technique, was used to characterize the elemental composition of the calcined mesoporous silicas. It demonstrated that the main components were Si and O (%), which confirmed the formation of silica in all the synthesized mesoporous silica cases. Its quantitative analysis also confirmed Rh(1 wt%) in the mesoporous silica supports.

3.1.2. XRD analysis

Low-angle XRD analysis of the synthesized samples indicated that the mesoporous MCM-41 molecular sieve showed the relative peaks to the (1 0 0), (1 1 0), (2 0 0) and (2 1 0) planes, corresponding to a hexagonal structure with symmetry P6 for the reflection planes (*h k* 0), as shown in Fig. 2(a). However, SBA-15-C has 2-dimensional (2D) hexagonal mesoporous channels which are interconnected through microporous spacers, and its characteristics peaks were reflected at the (1 0 0), (1 1 0) and (2 0 0) planes, associated with the p6mm hexagonal symmetry, as shown in Fig. 2(c). The SBA-15-S shown in Fig. 2(e) also shows a similar structure to SBA-15-C, as its characteristics peaks were observed at (1 0 0) and (1 1 0). However, the low-angle XRD pattern of the calcined KIT-6 shown in Fig. 2(g) shows a sharp intense peak corresponding to the (2 1 1) plane and a hump for the (2 2 0) plane. The XRD pattern clearly indicates that the material is well ordered mesoporous and belongs to the bicontinuous cubic space group, *Ia3d*, it is in good agreement with literature and suggests that mesoporous silica is KIT-6 with body centred cubic symmetry [23].

After calcination, the mesoporous silica material supported Rh catalysts were examined by means of long-angle XRD in the region where the rhodium or rhodium oxide peaks appeared. However, no distinct XRD peak was observed in this region for any of the catalysts shown in Fig. 2((b, d, f and h)). It emerged that rhodium oxide

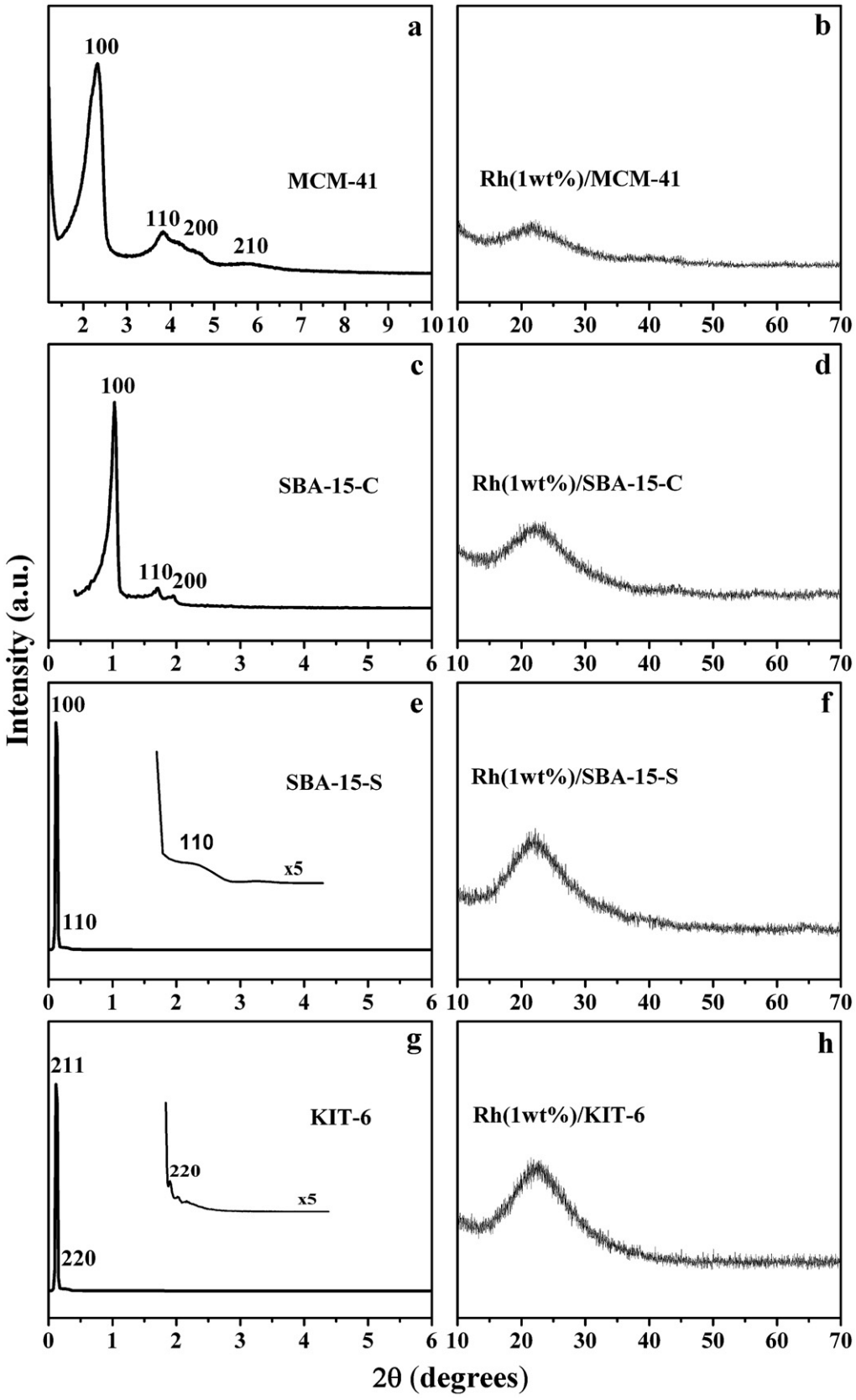

Fig. 2. Small and large angle XRD patterns of mesoporous silica support materials showing structure and Rh dispersion: (a) MCM-41, (b) Rh(1 wt%)/MCM-41, (c) SBA-15-C, (d) Rh(1 wt%)/SBA-15-C, (e) SBA-15-S, (f) Rh(1 wt%)/SBA-15-S, (g) KIT-6, (h) Rh(1 wt%)/KIT-6.

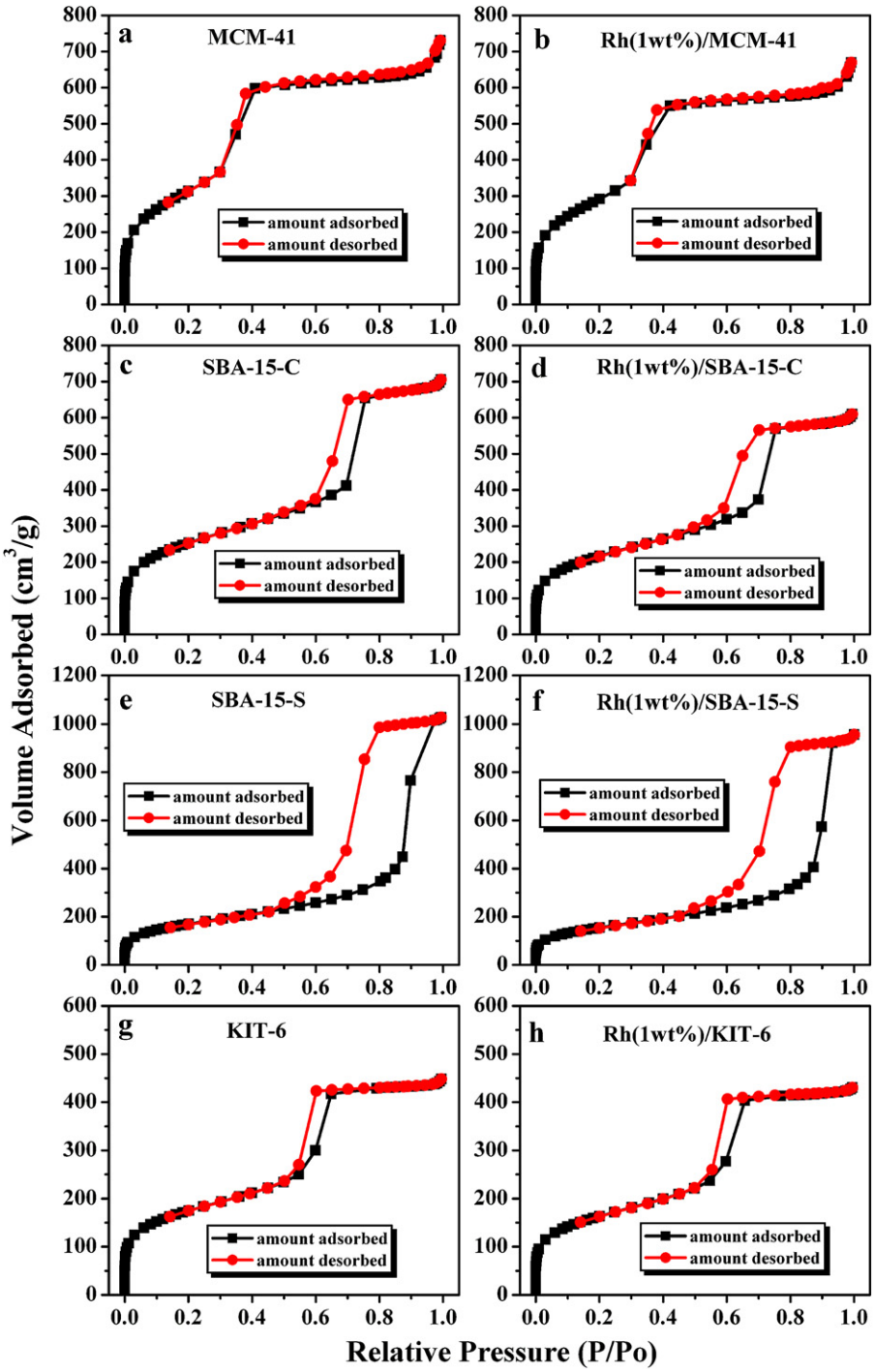

Fig. 3. Confirmation of different mesoporous silica materials and the effect of Rh incorporation by respective isotherms: (a) MCM-41, (b) Rh/MCM-41, (c) SBA-15-C, (d) Rh/SBA-15-C, (e) SBA-15-S, (f) Rh/SBA-15-S, (g) KIT-6, (h) Rh/KIT-6.

was well dispersed and probably present as a monolayer due to the low loading of 1 wt%, or the particle size was below the coherence length of the X-ray scattering.

3.1.3. N_2 sorption analysis

The porous and textural properties of the mesoporous silica and their supported Rh catalysts were examined by means of N_2 adsorption–desorption isotherms at 77 K, as shown in Fig. 3. All the mesoporous silica materials showed the typical type IV curves of mesoporous materials. Apart from MCM-41, the other three mesoporous silica materials, especially SBA-15-S, showed a sharp inflection at a relative pressure in the 0.6–0.9 range, which is indicative of a high quality mesoporous material with uniform mesopores [25]. However, in the case of MCM-41 this range was 0.35–0.45. No changes were detected in the nature of the isotherms or in the shapes of the hysteresis loops, indicating that the supports pore structure was preserved after Rh loading. However, some reduction in the heights of the hysteresis loops was observed in Rh/MCM-41, Rh/SBA-15-C and Rh/KIT-6, but no significant decrease in Rh/SBA-15-S appeared. This might be due to the fact that the introduced Rh occupied some of the pores of MCM-41, SBA-15-C and KIT-6, which reduced the adsorption of N_2 inside the pores. However, as shown

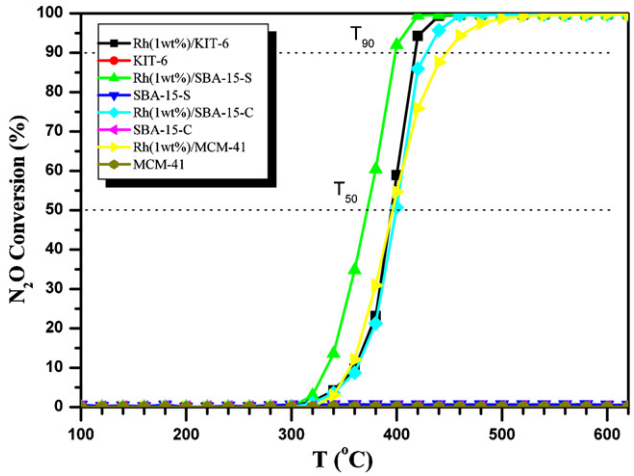

Fig. 4. Comparison of N_2O abatement by different mesoporous silica and their Rh(1 wt%) supported catalysts at specific reaction conditions: temperature = 100–620 °C, W/F = 5.10^{-4} g min/N ml, N_2O = 1700 ppm, GHSV = 26,500 h^{-1}.

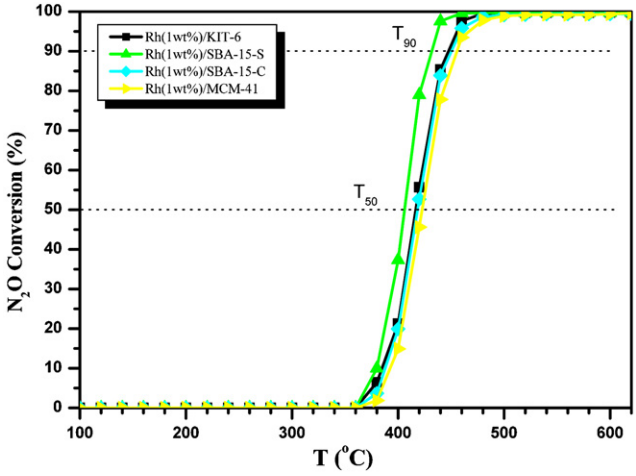

Fig. 5. Stability comparison of the one time used mesoporous silica supported Rh catalysts at specific reaction conditions: temperature = 100–620 °C, W/F = 5 × 10^{-4} g min/N ml, N_2O = 1700 ppm, GHSV = 26,500 h^{-1}.

in Fig 3, this was not so severe in SBA-15-S, and this might be due to its very large pores.

The textural properties obtained by N_2 sorption of the mesoporous silica and its Rh supported catalysts are shown in Table 1. The mesoporous materials have shown a large S_{BET} and PV. However, a notable decrease was observed in S_{BET} and PV after Rh impregnation, especially in MCM-41 and SBA-15-C, due to their hexagonal 1-dimensional or 2-dimensional (1D/2D) pore structures. This decrease in S_{BET} and PV of the materials might have been caused by a partial blockage of the pores by Rh or a partial collapse of the mesoporous structure [25]. A minor decrease was noticed after Rh loading in the S_{BET} and PV of SBA-15-S and KIT-6. This might be due to the fact that SBA-15-S has very large pores, with APD = 18 nm, compared to all the other supports, as shown in Table 1, and this leads to a better access for Rh diffusion and dispersion. However, KIT-6 has the advantage of having a 3-dimensional (3D) pore structure, which makes Rh diffusion and dispersion easy. A similar decreasing trend was also observed in S_{BET} and PV after using catalysts for 20 h. However, the SBA-15-S and KIT-6 support materials maintained their APD, compared to MCM-41 or SBA-15-C, even after 20 h of reaction.

3.2. N_2O abatement over mesoporous silica supported Rh catalysts

3.2.1. Support effect

The N_2O decomposition activities of the bare mesoporous silica supports and their Rh supported catalysts are shown in Fig. 4 at different temperatures. None of the parent mesoporous silica support materials show activity, which implies that no thermal decomposition of N_2O occurred in the temperature range of these experiments. Fig. 4 also shows that N_2O could be substantially decomposed in the presence of Rh on the mesoporous silica supports, and that the conversion level of the decomposition of N_2O increased with an increase in the reaction temperature. The highest activity of the catalysts was obtained for Rh/SBA-15-S (T_{50} = 372 °C, T_{90} = 398 °C). Rh/MCM-41 showed the lowest (T_{50} = 400 °C, T_{90} = 448 °C) activity of all. Rh/KIT-6 has higher activity (T_{50} = 394 °C, T_{90} = 417 °C) than Rh/SBA-15-C (T_{50} = 396 °C, T_{90} = 429 °C) and Rh/MCM-41, but slightly lower activity than Rh/SBA-15-S. The higher activity of Rh/SBA-15-S might be due to the fact that SBA-15 has a larger pore size than the others, which allows better access and diffusion of Rh, which leads to a better dispersion and distribution. Larger pores also allows the reactant better access to the active sites, hence better activity [8,26]. However, a mesoporous silica, like MCM-41, with smaller pores and a one dimensional pore structure might suffer from pore blockage problems due to the sintering of Rh at a higher temperature for N_2O decomposition [8]. This was also observed in the N_2 sorption results (Table 1), which showed a clear decrease in S_{BET}, PV and APD. The better activity performance of Rh/KIT-6 than Rh/MCM-41 or Rh/SBA-15-C might be due to its 3-dimensional pore structure, which reduces the risk of blockage due to metal agglomeration by sintering at a higher temperature and facilitates the transport of the reactant and product molecules [23]. As shown in Fig. 4, the difference in activity of the supported Rh catalysts can be seen more clearly at higher temperatures (in the region 350–450 °C), which is due to the diffusional effect of the different mesoporous support materials.

3.2.2. Deactivation and stability of the catalysts

One-time used mesoporous silica supported Rh catalysts have been retested for N_2O decomposition to examine the stability and deactivation phenomenon of the catalysts, as shown in Fig. 5. It was observed that Rh/SBA-15-S showed stability and no apparent deactivation was detected. A small decrease in the activity of Rh/KIT-6 (T_{90} = 447 °C) was found, compared to the fresh Rh/KIT-6 (T_{90} = 417 °C), which means it retained its structure. However, a significant decrease was observed in the activity of the used Rh/SBA-15-C and Rh/MCM-41 catalysts compared to the fresh catalysts. This might be due to the presence of micropores in the SBA-15-C structure that connect the mesoporous hexagonal framework, and which blocked the channel. The partial blockage due to sintering of Rh at a high temperature by 2D/1D pore structure could also be another reason for the deactivation of the Rh/SBA-15-C and Rh/MCM-41 catalysts.

3.2.3. Long-term stability of the catalysts

Long-term catalysts stability is an important criterion for potential catalyst in industrial applications. Long-term stability of the mesoporous silica Rh catalysts was observed when a continuous supply of N_2O (1700 ppm) was provided at the specific conditions shown in Fig. 6 for a time span of 20 h and T = 430 °C. Rh/SBA-15-S showed very good stability and only a very low concentration of N_2O (<20 ppm) was observed after the reaction, compared to the inlet concentration of 1700 ppm. In the case of Rh/KIT-6, the N_2O concentration after the reaction was maximum up to 220 ppm, as shown in Fig. 6. However, Rh/SBA-15-C and Rh/MCM-41 were not

Table 1
Physical properties of mesoporous materials supports and Rh supported catalysts by BET analysis, metal dispersion by CO-chemisorption and average Rh particle size by TEM/FE-SEM.

BET/Porosimetry				CO-chemisorption	TEM/FE-SEM
Support materials/supported catalysts	S_{BET} (m^2/g)	PV (cm^3/g)	APD (nm)	Rh dispersion (%)	Rh particle size (d_m, nm)
MCM-41	1135	1.219	3.2	–	–
SBA-15-C	878	1.078	5.3	–	–
SBA-15-S	596	1.603	18.0	–	–
KIT-6	602	0.735	4.8	–	–
Rh(1 wt%)/MCM-41	1060	1.020	3.1	44	2
Rh(1 wt%)/SBA-15-C	755	0.992	5.1	48	1.75
Rh(1 wt%)/SBA-15-S	545	1.467	17.5	72	0.8
Rh(1 wt%)/KIT-6	567	0.702	4.9	60	1.2
Rh(1 wt%)/MCM-41 (used;20 h)	830	0.813	2.9	–	–
Rh(1 wt%)/SBA-15-C (used; 20 h)	499	0.601	4.7	–	–
Rh(1 wt%)/SBA-15-S (used; 20 h)	509	1.420	17.1	–	–
Rh(1 wt%)/KIT-6 (used; 20 h)	515	0.603	4.8	–	–

stable (especially Rh/SBA-15-C) for the long-term period of 20 h. Rh/MCM-41 allowed 380 ppm of un-reacted N_2O to pass after the reaction at the end time of 20 h, whereas Rh/SBA-15-C had the highest value (606 ppm) at the end time of 20 h and was still showing a linear deactivation trend. The reasons for the stability and instability of SBA-15-S and SBA-15-C, have already been explained in the previous sections. Table 1 shows the textural properties of these catalysts after the 20 h long-term stability test, which are consistent with the reaction results shown in Fig. 6.

3.2.4. *Effect of oxygen on the catalysts activity*

The presence of 2–4% of oxygen in the exit flu gas from nitric acid plants associated with N_2O, has been reported to be the most inhibiting agent of N_2O decomposition [8,27]. It was confirmed that the inhibition was caused by reversible adsorption of oxygen onto surface sites [28]. It was noticed that the conversion of N_2O was decreased by introduction of oxygen, and the activity was recovered by removal of oxygen from the feed stream. Satsuma et al. [29] showed that the decrease in the nitrous oxide decomposition caused by oxygen was larger on the metal oxides having lower heat of formation. They also observed this phenomenon at different temperatures. The heat of formation was regarded as an indicator of metal–oxygen bond, hence the inhibitory effect of oxygen was correlated to the strength of the metal-oxygen bond.

The mechanism of N_2O decomposition over oxide catalysts involves a redox process as depicted in several kinetic studies [3]. This is described by the following four equations (* = chemisorption site):

$$N_2O + * \rightarrow N_2 + O*(k_1) \quad (1)$$

$$O_2 + 2* \rightarrow 2O*(k_2) \quad (2)$$

$$2O* \rightarrow O_2 + 2*(k'_2) \quad (3)$$

$$O* + N_2O \rightarrow N_2 + O_2 + *(k_3) \quad (4)$$

The catalyst surface can be oxidized either by a molecule of N_2O according to Eq. (1) (prevailing at very low oxygen pressure) or by chemisorption of molecular oxygen from gaseous phase according to Eq. (2) (dominating at high oxygen pressure). The reduction of the catalyst surface is proposed to follow the Eley–Rideal mechanism (Eq. (4)) or, alternatively, two adsorbed oxygen atoms can recombine according to Langmuir–Hinshelwood mechanism (Eq. (3)). Most of the kinetic models are based on the Langmuir–Hinshelwood mechanism, assuming that the surface concentration of the adsorbed oxygen is given by the adsorption equilibria (Eqs. (2) and (3)). The oxygen inhibition occurs indeed when the rate of oxygen removal from the catalyst surface is slower ($k_1 > k_3$).

The effect of O_2 on the mesoporous silica supported Rh catalysts for N_2O decomposition is shown in Fig. 7, and compared with the mesoporous silica supported Rh catalysts without O_2 and Uhde commercial catalysts for N_2O [4,30] in Table 2. As can be seen, O_2 inhibited all the catalysts unlike the catalysts

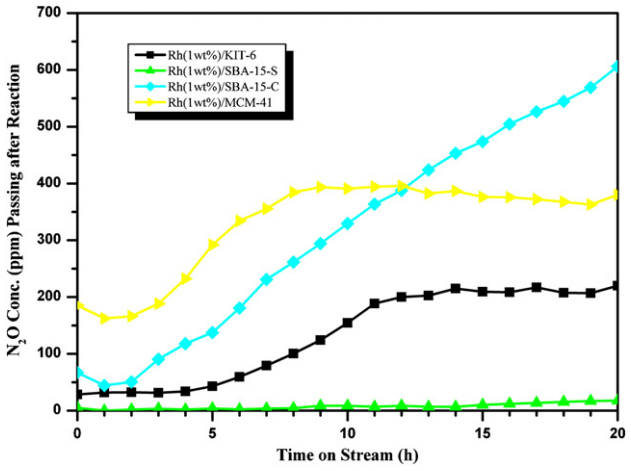

Fig. 6. Long term stability/deactivation of the mesoporous silica supported Rh catalysts at specific reaction condition: temperature = 430 °C, time = 20 h, W/F = 5×10^{-4} g min/N ml, N_2O feed conc. = 1700 ppm, GHSV = 26,500 h^{-1}.

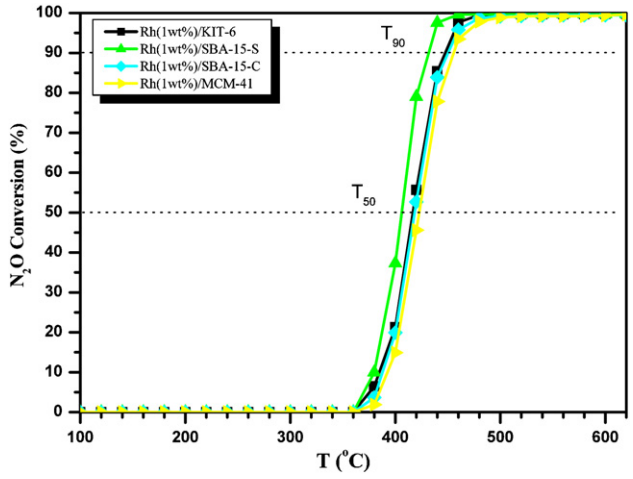

Fig. 7. Effect of O_2 on the decomposition of N_2O by the mesoporous silica supported Rh catalysts at specific reaction conditions: temperature = 100–620 °C, W/F = 5. $\times 10^{-4}$ g min/N ml, N_2O = 1700 ppm, O_2 = 5 vol.%, GHSV = 26,500 h^{-1}.

Table 2
Effect of O_2 on N_2O decomposition of mesoporous materials supported Rh catalysts.

Samples/Properties	No O_2-T_{50} (°C)	O_2-T_{50} (°C)	No O_2-T_{90} (°C)	O_2-T_{90} (°C)
Rh(1 wt%)/MCM-41	400	423	448	456
Rh(1 wt%)/SBA-15-C	396	419	429	451
Rh(1 wt%)/SBA-15-S	372	406	398	431
Rh(1 wt%)/KIT-6	394	417	417	447
Iron/Zeolite(Uhde) Ref. [28]	-	470	–	500

without O_2, however the order of the activity remained the same as it was without oxygen. The activity trend at 50% N_2O conversion was Rh/SBA-15-S (T_{50} = 406 °C) > Rh/KIT-6 (T_{50} = 417 °C) > Rh/SBA-15-C (T_{50} = 419 °C) > Rh/MCM-41 (T_{50} = 423 °C) > Fe/Zeolite Uhde (T_{50} = 470 °C), and the trend at 90% N_2O conversion was also Rh/SBA-15-S (T_{90} = 431 °C) > Rh/KIT-6 (T_{90} = 447 °C) > Rh/SBA-15-C (T_{90} = 451 °C) > Rh/MCM-41 (T_{90} = 456 °C) > Fe/Zeolite Uhde (T_{90} = 500 °C). However, a point worth mentioning is that even the worst mesoporous silica supported Rh catalyst showed a better activity than the commercial catalyst.

3.3. Rhodium vs. rhodium oxide over mesoporous silica supports for N_2O abatement

The difference in activity of the Rh oxide and the reduced Rh supported on the mesoporous silica for N_2O decomposition at 95% conversion (T_{95}, °C) has been shown in Fig. 8. It can be noticed that the mesoporous silica supported Rh oxide catalysts showed 95% conversion of N_2O at a lower temperature than the mesoporous silica supported reduced Rh catalysts. It has already been reported [19] that Rh has a better activity than other metals for N_2O decomposition in both oxide or reduced form. However, the Rh oxide is more active on the mesoporous silica supported Rh catalysts shown here than the reduced Rh.

XPS spectra with deconvolution results of the mesoporous silica (KIT-6, SBA-15-C and SBA-15-S) supported Rh catalysts were analyzed qualitatively and quantitatively in order to correlate the above results. Fig. 9 shows the Rh 3d XPS spectra of the mesoporous silica supported Rh catalysts and the results regarding the curves deconvolution are presented in Table 3. It had been found in literature [31–36] on the basis of Rh $3d_{5/2}$ XPS analysis, that reduced Rh (Rh^0) shows its characteristic peaks at 307.1 eV, or below, Rh oxide with a non stoichiometric state or Rh(I) at 308 eV,

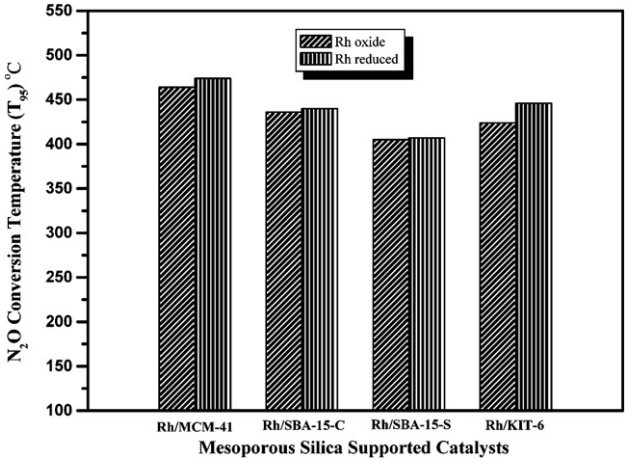

Fig. 8. N_2O abatement (T_{95} °C) comparison by Rh oxide vs. Rh reduced supported on the different mesoporous silica supports at specific reaction conditions: W/F = 5×10^{-4} g min/N ml, N_2O = 1700 ppm, GHSV = 26,500 h^{-1}.

Table 3
Binding energy values (eV) and atomic concentrations (%) of Rh $3d_{5/2}$ by XPS.

Catalyst	Rh^0	Rh^{+1}	Rh^{3+}
1%Rh/KIT 6	307.1 (20.3)	308.5 (65.3)	310.0 (14.4)
1%Rh/SBA-15-C	307.2 (22.4)	308.7 (67.8)	310.0 (9.8)
1%Rh/SBA-15-S	307.2 (7.7)	308.9 (82.8)	309.9 (9.5)

or higher, and Rh(III) at 309 eV, or higher. The results shown in Fig. 9 and presented in Table 3 show that Rh is found in different oxidation states and the positions of the Rh^0, Rh(I) and Rh(III) are consistent with the above mentioned literature. However, the results pointed out that the mesoporous silica supported Rh

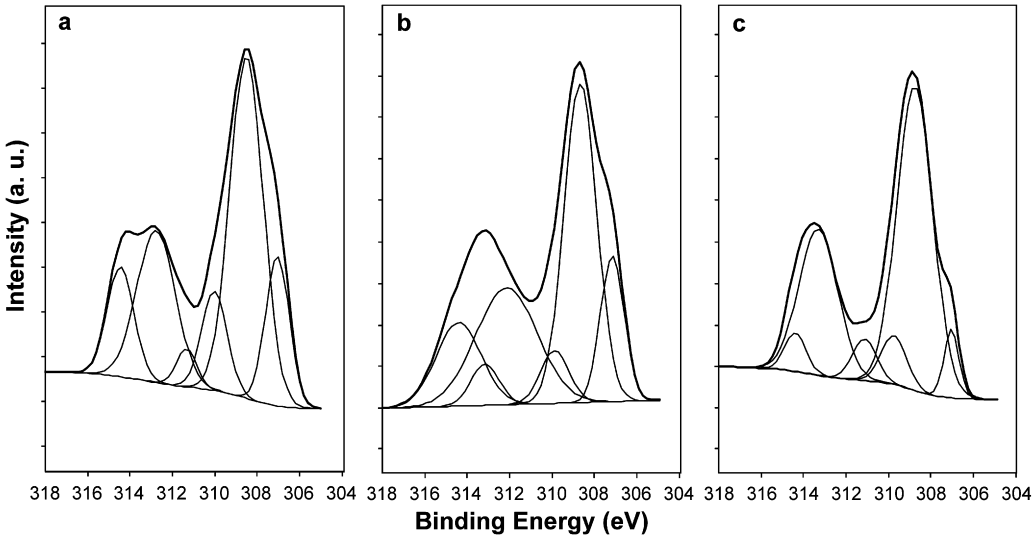

Fig. 9. Rh 3d XPS spectra of (a) Rh/KIT-6, (b) Rh/SBA-15-C, and (c) Rh/SBA-15-S showing different oxidation states of Rh.

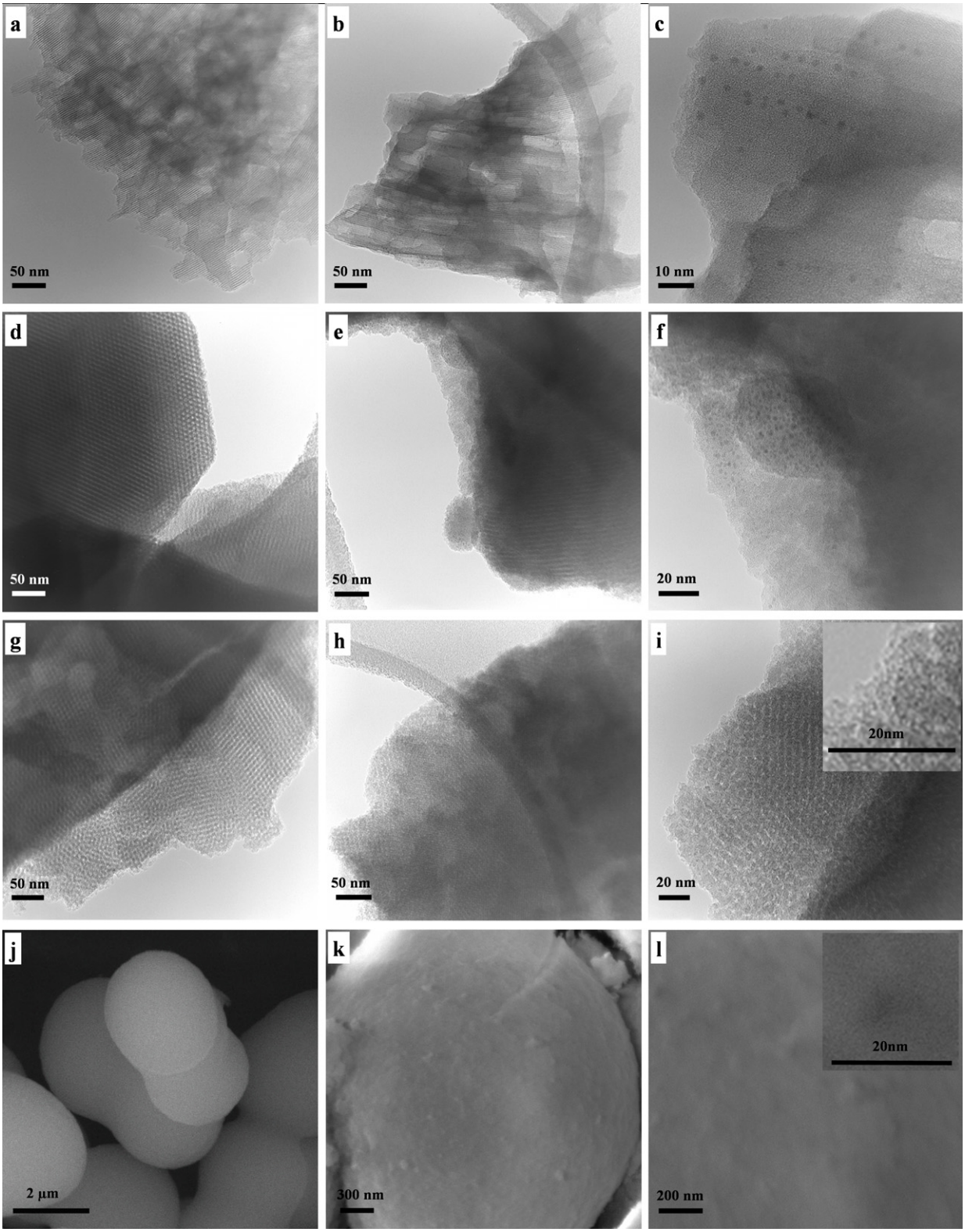

Fig. 10. TEM images of MCM-41, SBA-15-C, KIT-6 and their supported Rh catalysts, and FE-SEM of SBA-15-S and Rh/SBA-15-S showing the support materials structure and Rh distribution.

catalysts showed more Rh^{+1} percentage than Rh^0 or Rh^{+3} (Table 1). This means that the main activity of the supported Rh catalysts is mainly due to Rh^{+1}. 1 wt% Rh/SBA-15-S showed a higher percentage of Rh^{+1} (82.8) than Rh/SBA-15-C (67.8) and Rh/KIT-6 (65.3), a result that is also consistent with the previously discussed activity results for N_2O decomposition.

3.4. Effect of rhodium size and dispersion on the mesoporous silica supports for N_2O abatement

The TEM images of the mesoporous silicas (MCM-41, SBA-15-C, KIT-6) and their Rh supported catalysts are shown in Fig. 10. The support materials confirm the ordered mesostructures which

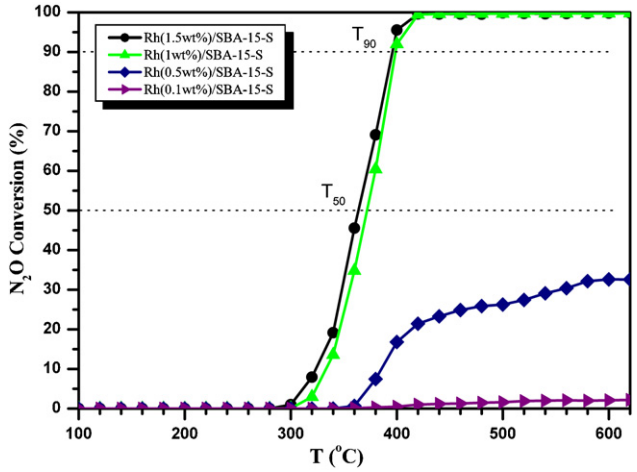

Fig. 11. Effect of Rh wt% on SBA-15-S for the decomposition of N_2O at specific reaction conditions: temperature = 100–620 °C, W/F = 5×10^{-4} g min/N ml, N_2O = 1700 ppm, GHSV = 26,500 h^{-1}.

appear to be conserved, even after Rh loading. It can also be noticed that the metal is uniformly distributed, in agreement with the XRD results reported in Section 3.1.2. No TEM images of SBA-15-S or its Rh supported catalyst could be obtained due to its high particle charge affinity. FE-SEM images were therefore obtained, as shown in Fig. 10, in order to observe the metal distribution.

The Rh particle size was obtained on the different mesoporous silicas from the TEM and FE-SEM results and is shown in Table 1. The Rh on SBA-15-S showed a smaller particle size than the other supported catalysts. The catalytic activity and the average particle size of the Rh on the mesoporous silicas followed the same trend, that is, the smaller the Rh size, the higher the catalytic activity [17].

The smaller Rh particle size on SBA-15-S also favoured metal dispersion, as shown in Table 1. SBA-15-S has slightly higher dispersion than the other supported catalysts, and this result is in line with the FE-SEM and activity results.

3.5. *Effect of rhodium loading on the optimized mesoporous silica support for N_2O abatement*

Fig. 11 shows that N_2O could be substantially decomposed in the presence of Rh on SBA-15-S and the conversion level for the decomposition of N_2O increased with the increase of the temperature. It has been observed that the catalytic activity increased as the Rh loading increased from 0.1 to 1.5 wt%. It has been reported [6] that N_2O decomposition activity is more sensitive to Rh loading, where Rh catalyst with a high loading of 5% supported on Al-SBA-15, showed the best activity for N_2O decomposition. However, the output activity was not comparable to the increased Rh loading. Therefore, to economics point of view, Rh loading has been limited here up to 1.5 wt%. The increased activity of Rh(1.5 wt%)/SBA-15-S for N_2O decomposition here might be due to the increased metal with good distribution and higher dispersion. However the difference in activity between 1 and 1.5 wt% supported catalysts is not good enough as compared to the increased amount of expensive Rh. Low loading of 0.1 wt% Rh showed negligible activity. It might be possible that very low content went into the deep internal structure, was trapped, and not available to the reactants for the reaction.

4. Conclusions

Different mesoporous silica materials (MCM-41, SBA-15-C, SBA-15-S, and KIT-6) have been synthesized and used as support materials for Rh catalysts to perform N_2O decomposition. Rh/SBA-15-S not only showed the highest activity for N_2O decomposition, but also a better strength towards ageing compared to all the other catalysts. Moreover, Rh/SBA-15-S has shown a superior performance in the presence of O_2 as the inhibiting agent. The larger pore size of SBA-15-S in Rh/SBA-15-S may favour a better Rh access, diffusion and dispersion, and therefore lead to a higher activity. Furthermore, the higher metal dispersion due to the smaller Rh particle size and the formation of more Rh^{+1} than Rh^0 or Rh^{+3} on the SBA-15-S, compared to other supports, also favoured a higher N_2O decomposition. The long-term stability of Rh/SBA-15-S at 430 °C for 20 h, with better preserved support characteristics than the other catalysts studied here, indicates its suitability to be optimized in further research and future applications.

Acknowledgements

M. Hussain is grateful to the Regione Piemonte and the Politecnico di Torino, Italy for his post-doctoral fellowship grant.

References

[1] W.B. Tolman, Binding and activation of N_2O at transition-metal centers: recent mechanistic insights, Angew. Chem. Int. Ed. 49 (2010) 1018–1024.
[2] J.C. Kramlich, W.P. Linak, Nitrous oxide behavior in the atmosphere, and in combustion and industrial systems, Prog. Energy Combust. Sci. 20 (1994) 149–202.
[3] F. Kapteijn, J. Rodriguez-Mirasol, J.A. Moulijn, Heterogeneous catalytic decomposition of nitrous oxide, Appl. Catal. B 9 (1996) 25–64.
[4] J. Perez-Ramirez, F. Kapteijn, K. Schoffel, J.A. Moulijn, Formation and control of N_2O in nitric acid production: where do we stand today? Appl. Catal. B 44 (2003) 117–151.
[5] V.N. Parmon, G.I. Panov, A. Uriarte, A.S. Noskov, Nitrous oxide in oxidation chemistry and catalysis: application and production, Catal. Today 100 (2005) 115–131.
[6] X. Xu, H. Xu, F. Kapteijn, J.A. Moulijn, SBA-15 based catalysts in catalytic N_2O decomposition in a model tail-gas from nitric acid plants, Appl. Catal. B 53 (2004) 265–274.
[7] J. Du, W. Kuang, H. Xu, W. Shen, D. Zhao, The influence of precursors on Rh/SBA-15 catalysts for N_2O decomposition, Appl. Catal. B 84 (2008) 490–496.
[8] S. Kawi, S.Y. Liu, S.-C. Shen, Catalytic decomposition and reduction of N_2O on Ru/MCM-41 catalyst, Catal. Today 68 (2001) 237–244.
[9] M.N. Debbagh Boutarbouch, J.M. Garcia Cortes, M.S. Soussi El Begrani, C. Salinas Martinez de Lecea, J. Perez-Ramirez, Catalytic conversion of N_2O over FeZSM-5 zeolite in the presence of CO and NO, Appl. Catal. B 54 (2004) 115–123.
[10] P. Granger, P. Esteves, S. Kieger, L. Navascues, G. Leclercq, Effect of yttrium on the performances of zirconia based catalysts for the decomposition of N_2O at high temperature, Appl. Catal. B 62 (2006) 236–243.
[11] S. Suarez, M. Yates, A.L. Petre, J.A. Martin, P. Avila, J. Blanco, Development of a new Rh/TiO_2–sepiolite monolithic catalyst for N_2O decomposition, Appl. Catal. B 64 (2006) 302–311.
[12] N. Russo, D. Mescia, D. Fino, G. Saracco, V. Specchia, N_2O decomposition over perovskite catalysts, Ind. Eng. Chem. Res. 46 (2007) 4226–4231.
[13] B.M. Abu-Zied, W. Schwieger, A. Unger, Nitrous oxide decomposition over transition metal exchanged ZSM-5 zeolites prepared by the solid-state ion-exchange method, Appl. Catal. B 84 (2008) 277–288.
[14] G. Giecko, T. Borowiecki, W. Gac, J. Kruk, Fe_2O_3/Al_2O_3 catalysts for the N_2O decomposition in the nitric acid industry, Catal. Today 137 (2008) 403–409.
[15] K. Asano, C. Ohnishi, S. Iwamoto, Y. Shioya, M. Inoue, Potassium-doped Co_3O_4 catalyst for direct decomposition of N_2O, Appl. Catal. B 78 (2008) 242–249.
[16] Q. Shen, L. Li, J. Li, H. Tian, Z. Hao, A study on N_2O catalytic decomposition over Co/MgO catalysts, J. Hazard. Mater. 163 (2009) 1332–1337.
[17] S. Parres-Esclapez, F.E. Lopez-Suarez, A. Bueno-Lopez, M.J. Illan-Gomez, B. Ura, J. Trawczynski, Rh–Sr/Al_2O_3 catalyst for N_2O decomposition in the presence of O_2, Top. Catal. 52 (2009) 1832–1836.
[18] S. Sklenak, P.C. Andrikopoulos, B. Boekfa, B. Jansang, J. Nováková, L. Benco, T. Bucko, J. Hafner, J. Dedecek, Z. Sobalík, N_2O decomposition over Fe-zeolites: structure of the active sites and the origin of the distinct reactivity of Fe-ferrierite, Fe-ZSM-5, and Fe-beta. A combined periodic DFT and multispectral study, J. Catal. 272 (2010) 262–274.
[19] T.P. Gaidei, Nitrous oxide: properties, producing, grounds of manipulations, and fields of application, Russ. J. Appl. Chem. 82 (2009) 1689–1705.
[20] M. Hussain, S.-K. Song, J.-H. Lee, S.-K. Ihm, Characteristics of CoMo catalysts supported on modified MCM-41 and MCM-48 materials for thiophene hydrodesulfurization, Ind. Eng. Chem. Res. 45 (2006) 536–543.
[21] J.G. Park, C.H. Ko, K.B. Yi, J.-H. Park, S.-S. Han, S.-H. Cho, J.-N. Kim, Reactive adsorption of sulfur compounds in diesel on nickel supported on mesoporous silica, Appl. Catal. B 81 (2008) 244–250.
[22] L. Wang, T. Qi, Y. Zhang, J. Chu, Morphosynthesis route to large-pore SBA-15 microsphere, Microporous Mesoporous Mater. 91 (2006) 156–160.

[23] K. Soni, B.S. Rana, A.K. Sinha, A. Bhaumik, M. Nandi, M. Kumar, G.M. Dhar, 3-D ordered mesoporous KIT-6 support for effective hydrodesulfurization catalysts, Appl. Catal. B 90 (2009) 55–63.
[24] W. Dai, M. Zheng, Y. Zhao, S. Liao, G. Ji, J. Cao, Template synthesis of three-dimensional cubic ordered mesoporous carbon with tunable pore sizes, Nanoscale Res. Lett. 5 (2010) 103–107.
[25] M.K. Gnanamani, G. Jacobs, U.M. Graham, W. Ma, V.R.R. Pendyala, M. Ribeiro, B.H. Davis, Studies on KIT-6 supported cobalt catalyst for fischer–tropsch synthesis, Catal. Lett. 134 (2010) 37–44.
[26] M. Hussain, J.S. Yun, S.-K. Ihm, N. Russo, F. Geobaldo, Synthesis, characterization, and thiophene hydrodesulfurization activity of novel macroporous and mesomacroporous carbon, Ind. Eng. Chem. Res. 50 (2011) 2530–2535.
[27] A.G. Anshits, E.V. Kondratenko, E.N. Voskresenskaya, L.I. Kurteeva, N.I. Pavlenko, The influence of O_2 on oxidative coupling of methane over oxide catalysts using N_2O as oxidant, Catal. Today 46 (1998) 211–216.
[28] A. Satsuma, H. Maeshima, K. Watanabe, K. Suzuki, T. Hattori, Effect of methane and oxygen on decomposition of nitrous oxide over metal oxide catalysts, Catal. Today 63 (2000) 347–353.
[29] A. Satsuma, H. Maeshima, K. Watanabe, T. Hattori, Effect of oxygen on decomposition of nitrous oxide over various metal oxide catalysts, Energy Convers. Manage. 42 (2001) 1997–2003.
[30] M. Groves, R. Maurer, M. Schwefer, R. Siefert, Abatement of N_2O and NO_x emission from nitric acid plants with the Uhde EnviNOx process, in: Nitrogen 2006 International Conference, Vienna, Austria, 2006.
[31] A. Bueno-Lopez, I. Such-Basanez, C. Salinas-Martinez de Lecea, Stabilization of active Rh_2O_3 species for catalytic decomposition of N_2O on La-, Pr-doped CeO_2, J. Catal. 244 (2006) 102–112.
[32] Y. Wang, Z. Song, D. Ma, H. Luo, D. Liang, X. Bao, Characterization of Rh-based catalysts with EPR, TPR, IR and XPS, J. Mol. Catal. A-Chem. 149 (1999) 51–61.
[33] S. Suhonen, R. Polvinen, M. Valden, K. Kallinen, M. Harkonen, Surface oxide on supported Rh particles: thermal decomposition of Rh oxide under high vacuum conditions, Appl. Surf. Sci. 200 (2002) 48–54.
[34] K. Polychronopoulou, J.L.G. Fierro, A.M. Efstathiou, The phenol steam reforming reaction over MgO-based supported Rh catalysts, J. Catal. 228 (2004) 417–432.
[35] J.F. Munera, S. Irusta, L.M. Cornaglia, E.A. Lombardo, D.V. Cesar, M. Schmal, Kinetics and reaction pathway of the CO_2 reforming of methane on Rh supported on lanthanum-based solid, J. Catal. 245 (2007) 25–34.
[36] Y.V. Larichev, O.V. Netskina, O.V. Komova, V.I. Simagina, Comparative XPS study of Rh/Al_2O_3 and Rh/TiO_2 as catalysts for $NaBH_4$ hydrolysis, Int. J. Hydrogen Energy 35 (2010) 6501–6507.